RESEARCH ARTICLE

The yeast oligopeptide transporter Opt2 is localized to peroxisomes and affects glutathione redox homeostasis

Yael Elbaz-Alon[1], Bruce Morgan[2], Anne Clancy[3,4], Theresa N.E. Amoako[2], Einat Zalckvar[1], Tobias P. Dick[2], Blanche Schwappach[3,4] & Maya Schuldiner[1]

[1]Department of Molecular Genetics, Weizmann Institute of Science, Rehovot, Israel; [2]Division of Redox Regulation, German Cancer Research Center (DKFZ), DKFZ-ZMBH Alliance, Heidelberg, Germany; [3]Department of Molecular Biology, University of Göttingen, Göttingen, Germany; and [4]Faculty of Life Sciences, University of Manchester, Manchester, UK

Correspondence: Maya Schuldiner, Weizmann Institute of Science, 234 Herzl St, Rehovot 7610001, Israel.
Tel.: 972 8 9346346; fax: 972 8 9346373; e-mail: maya.schuldiner@weizmann.ac.il

Received 1 May 2014; revised 8 July 2014; accepted 7 August 2014. Final version published online 22 September 2014.

DOI: 10.1111/1567-1364.12196

Editor: Guenther Daum

Keywords
glutathione homeostasis; GSH; GSSG; peroxisome; Grx1-roGFP2.

Abstract

Glutathione, the most abundant small-molecule thiol in eukaryotic cells, is synthesized *de novo* solely in the cytosol and must subsequently be transported to other cellular compartments. The mechanisms of glutathione transport into and out of organelles remain largely unclear. We show that budding yeast Opt2, a close homolog of the plasma membrane glutathione transporter Opt1, localizes to peroxisomes. We demonstrate that deletion of *OPT2* leads to major defects in maintaining peroxisomal, mitochondrial, and cytosolic glutathione redox homeostasis. Furthermore, Δ*opt2* strains display synthetic lethality with deletions of genes central to iron homeostasis that require mitochondrial glutathione redox homeostasis. Our results shed new light on the importance of peroxisomes in cellular glutathione homeostasis.

Introduction

The redox environment inside a cell is essential for maintaining normal protein activities as well as for protecting cells from the damaging effects of reactive oxygen species (ROS) produced either by cell metabolism or by external sources. Redox homeostasis in eukaryotic cells is thus highly regulated and achieved through the concerted function of a large number of enzymes and small molecules. Examples of such central players are glutaredoxins, thioredoxins, catalases, and peroxidases, as well as small antioxidant molecules such as glutathione (Grant, 2001; Herrero *et al.*, 2008; Lopez-Mirabal & Winther, 2008).

Glutathione (γ-glutamylcysteinylglycine) is the major small-molecule thiol-disulfide redox couple of most eukaryotic cells (cellular concentration of 1–11 mM). Glutathione is an essential metabolite in yeast (Grant *et al.*, 1996), potentially due to its role in iron metabolism (Kumar *et al.*, 2011). It performs diverse functions in catalysis, metabolism, transport, and detoxification and plays a crucial role in protecting cells from the damaging effect of ROS by serving as a co-factor for enzymes involved in antioxidant defense (Meister, 1988).

It appears important for cells to robustly regulate the amounts of reduced (GSH) and oxidized glutathione (GSSG) in a compartment-specific manner. The cytosol of yeast, for example, exhibits a glutathione redox potential (E_{GSH}) of *c.* −320 mV, which implies a GSH:GSSG ratio of *c.* 50 000 : 1, assuming a 10 mM total glutathione pool (Gutscher *et al.*, 2008; Braun *et al.*, 2010; Morgan *et al.*, 2011). This makes it much more reducing than the glutathione pool in the endoplasmic reticulum (ER), in which recent measurements with an ER-specific roGFP2-based sensor, indicate is *c.* −208 mV at pH 7.0 (Birk *et al.*, 2013). Presumably, the redox state of the glutathione pool is optimized for the specific range of biochemical processes present within each organelle. Each organelle likely maintains mechanisms to regulate the redox state of its glutathione pool independently of other compartments as well as the ability to transport both GSH and GSSG across intracellular membranes. Furthermore, kinetic separation ensures that the glutathione redox couple is not in thermodynamic equilibrium with other cellular redox couples. Consequently, it makes little sense to discuss an 'overall cellular redox state'. Instead, it is essential to study the regulation of individual redox

couples with subcellular compartment resolution, and the investigation of the redox communication between subcellular compartments is of prime interest.

Cellular glutathione pools are regulated by biosynthesis, degradation, uptake/excretion, interconversion between the reduced and oxidized forms and intracellular partitioning through organelle-specific transport systems. In addition to the GSH : GSSG ratio, total glutathione concentration must also be regulated as strong depletion or elevation of cytosolic glutathione levels has a toxic effect (Srikanth *et al.*, 2005; Kumar *et al.*, 2011). Glutathione can only be synthesized *de novo* in the cytosol and must, therefore, be transported into other subcellular compartments according to their specific requirements. Three different transporters are known to facilitate intracellular glutathione transport, all of which are localized in the vacuolar membrane: the ATP-binding cassette pumps Ycf1 (Li *et al.*, 1996; Rebbeor *et al.*, 1998; Morgan *et al.*, 2013) and Bpt1 (Klein *et al.*, 2002; Sharma *et al.*, 2002), and the major facilitator superfamily protein Gex1 (Dhaoui *et al.*, 2011). All three have been implicated in heavy metal detoxification through the transport of metal-glutathione conjugates from the cytosol into the vacuolar lumen. Gex1 is dually localized to the vacuolar and plasma membranes (PMs) and has also been postulated to mediate metal-coupled glutathione excretion out of the cell (Dhaoui *et al.*, 2011). Transport systems mediating GSH/GSSG transport across other intracellular membranes remain unidentified.

The recent development of genetically-encoded fluorescent redox probes has enabled specific measurement of the glutathione redox potential (E_{GSH}), with subcellular compartment resolution in living cells (comprehensively reviewed in Meyer & Dick, 2010). In the yeast *Saccharomyces cerevisiae* such probes have been used to measure glutathione redox changes in the cytosol (Braun *et al.*, 2010), nucleus (Dardalhon *et al.*, 2012), peroxisomes (Ayer *et al.*, 2012), and mitochondria (Kojer *et al.*, 2012). However, not all subcellular compartments have been investigated and much remains to be understood regarding the partitioning of cellular glutathione homeostasis.

In this study, we generate a peroxisome-targeted E_{GSH} sensor, Grx1-roGFP2-SKL, and use it to demonstrate that a previously uncharacterized protein, Opt2, which localizes specifically to peroxisomes, affects peroxisomal, cytosolic, and mitochondrial glutathione redox homeostasis.

Materials and methods

Plasmids, strains, and media

All yeast strains in this study are based on the BY4741/2 laboratory strains (Brachmann *et al.*, 1998). General laboratory strains and strains created in this study are listed in Table 1. All genetic manipulations were performed using the Li-acetate, PEG, ssDNA method for transforming yeast strains (Gietz & Woods, 2006) using integration plasmids previously described in (Longtine *et al.*, 1998; Janke *et al.*, 2004). Deletions were verified using PCR for loss of the endogenous gene copy.

Cultures were grown at 30 °C in either rich medium [1% Bacto-yeast extract (BD), 2% Bacto-peptone (BD), and 2% dextrose (Amresco)] or synthetic (SD) minimal medium [0.67% yeast nitrogen base without amino acids (Conda Pronadisa), and 2% dextrose containing the appropriate supplements for plasmid selection]. The antibiotics Nourseothricin (NAT; purchased from Werner BioAgents, Germany) and G418 (Calbiochem-Merck) were used at a final concentration of 200 μg mL^{-1} for selection where needed.

For assaying growth on solid media supplemented with GSH: Strains were grown ON at 30 °C in liquid minimal media, back-diluted to OD_{600} = 0.15 and allowed to grow until OD_{600} = 1, then serially diluted (10-fold) and spotted on SD agar plates containing GSH [SD + 2% agar supplemented with essential amino acid/adenine/uracil mix necessary for yeast growth and GSH (Sigma-Aldrich, Germany) to a final concentration of 250 μM].

For assaying growth on solid media containing oleic acid as a sole carbon source: Strains were grown ON at 30 °C in liquid SD media, back-diluted to OD_{600} = 0.016 and grown ON at 30 °C in liquid minimal media containing 0.3% glucose. The cells were then back-diluted to OD_{600} = 0.2, allowed to grow until OD_{600} = 0.5–1 and then serially diluted (10-fold) and spotted on YPO (0.32% Oleate/Tween40, 1% yeast extract, 2% bacto-peptone) or YNO (0.32% Oleate/Tween40, 0.67% YNB-w/o amino acids) plates.

Synthetic lethality screen of Δ*opt2* against the yeast deletion library

A synthetic genetic array (SGA) ready query strain harboring deletion of *opt2* (*his3Δ1 leu2Δ0 met15Δ0 ura3Δ0 can1Δ::STE2pr-spHIS5 lyp1Δ::STE3pr-LEU2 opt2Δ*::NAT^r) was constructed and mated against the yeast deletion library (Giaever *et al.*, 2002) using SGA techniques that allow efficient introduction of a trait (mutation or marker) into systematic yeast libraries. SGA was performed as previously described (Tong *et al.*, 2001; Tong & Boone, 2006; Cohen & Schuldiner, 2011). Briefly, using a RoToR bench-top colony arrayer (Singer Instruments) to manipulate libraries in high-density formats (1536), haploid strains from opposing mating types, each harboring a different genomic alteration, were mated on rich media plates. Diploid cells were selected on plates containing all

Table 1. List of yeast strains used in this study

Name	Mating type	Genetic background	Sources
BY4742	MATα	*his3Δ1 leu2Δ0 lys2Δ0 ura3Δ0*	Brachmann *et al.* (1998)
BY4741	MATa	*his3Δ1 leu2Δ0 met15Δ0 ura3Δ0*	Brachmann *et al.* (1998)
YMS893	MATα	BY4742 NAT^r::GPDp-GFP-Opt1	This study
YMS894	MATα	BY4742 NAT^r::GPDp-GFP-Opt2	This study
YMS839	MATa	BY4741 NAT^r::GPDp-GFP-Opt2	This study
YMS1330	MATα	BY4742 *opt1*Δ::NAT^r	This study
YMS1331	MATα	BY4742 *opt2*Δ::NAT^r	This study
YMS1332	MATα	BY4742 *cta1*Δ::KAN^r	This study
YMS1144	MATα	BY4742 *cta1*Δ::KAN^r *opt2*Δ::NAT^r	This study
YMS721	MATα	*his3Δ1 leu2Δ0 met15Δ0 ura3Δ0 can1Δ::STE2pr-spHIS5 lyp1Δ::STE3pr-LEU2*	Breslow *et al.* (2008)
YMS1334	MATα	YMS721 *opt2*Δ::NAT^r	This study
YMS070	MATα	Anp1-RFP::KAN^r	Huh *et al.* (2003)
YMS074	MATα	Chc1-RFP::KAN^r	Huh *et al.* (2003)
YMS072	MATα	Sec13-RFP::KAN^r	Huh *et al.* (2003)
YMS225	MATα	Pex3-RFP::KAN^r	Huh *et al.* (2003)
YMS203	MATα	Erg6-RFP::KAN^r	Huh *et al.* (2003)
YMS073	MATα	Cop1-RFP::KAN^r	Huh *et al.* (2003)
YMS903	Unknown	NAT^r::GPDp-GFP-Opt2 Chc1-RFP::KAN^r	This study, tetrad dissection
YMS904	Unknown	NAT^r::GPDp-GFP-Opt2 Sec13-RFP::KAN^r	This study, tetrad dissection
YMS905	Unknown	NAT^r::GPDp-GFP-Opt2 Pex3-RFP::KAN^r	This study, tetrad dissection
YMS906	Unknown	NAT^r::GPDp-GFP-Opt2 Erg6-RFP::KAN^r	This study, tetrad dissection
YMS907	Unknown	NAT^r::GPDp-GFP-Opt2 Anp1-RFP::KAN^r	This study, tetrad dissection
YMS908	Unknown	NAT^r::GPDp-GFP-Opt2 Cop1-RFP::KAN^r	This study, tetrad dissection
YMS1333	MATa	BY4741 gsh1Δ::KANr	Giaever *et al.* (2002)
YMS1720	MATa	BY4742 opt2Δ::KANr Pex3-Cherry::HIS^r	This study

selection markers found on both parent haploid strains. Sporulation was then induced by transferring cells to nitrogen starvation plates. Haploid cells containing all desired mutations were selected for by transferring cells to plates containing all selection markers alongside the toxic amino acid derivatives canavanine and thialysine (Sigma-Aldrich) to select against remaining diploids. Specifically, the SGA was performed as described for creating a library of haploid cells harboring a double deletion (*opt2*Δ::NAT^r *xxx*Δ::Kan^r) and scored for colonies that were absent after the final double-mutant selection to identify genes that display synthetic lethality with *opt2*Δ under nonstress conditions. In parallel, and to identify genes that display synthetic lethality with *opt2*Δ specifically under conditions of oxidative stress, 3 mM diamide (Sigma-Aldrich) was added to the haploid and double-mutant selection plates and colony sizes were re-measured.

Microscopy

Manual microscopy was performed using either one of two systems: For Fig. 1a and b, we used an Olympus IX71 microscope controlled by the DELTA VISION SOFTWORX 3.5.1 software with ×60 oil lens. Images were captured by a Photometrics Coolsnap HQ camera with excitation at 490/20 nm and emission at 528/38 nm (GFP) or excitation at 555/28 nm and emission at 617/73 nm (mCherry/RFP). Images were transferred to Adobe Photoshop CS3 for slight contrast and brightness adjustments.

For Fig. 3a, cells expressing Pex3-RFP from the genomic locus (Huh *et al.*, 2003), transformed with p415MET25 Grx1-roGFP2-SKL were grown overnight in selective media (synthetic dropout, -Leucine). Cells were imaged using the Deltavision microscope system (Applied Precision, Inc.) with a Coolsnap HQ2 CCDcamera (Roper Scientific) mounted on an Olympus IX71 microscope with an UPlanSApo 100×/1.40 oil objective. Filter sets of excitation at 475/28 nm and emission at 523/36 nm (GFP) or excitation 542/27 nm and emission 594/45 nm (RFP) were used, and images were processed using the SOFTWORX deconvolution software.

For Fig. 3b, Control or Δ*opt2* cells expressing Pex3-RFP or Pex3-cherry, respectively, from the genomic locus (Huh *et al.*, 2003) were transformed with a plasmid

bearing the Grx1-roGFP2-SKL probe. For each strain, 50 fields from three biological replicates (independent transformants) were imaged in three focal planes 2 μm apart from each other, where a bright-field image, the red and green fluorescence were recorded. An image-processing pipeline encompassing the following steps was assembled in KNIME (Tiwari & Sekhar, 2007). As described in Jonikas *et al.* (2009), subtraction of the top from the bottom bright-field image was used to automatically identify cells. In the identified cells (*c.* 300 per strain analyzed), the Red-signal was thresholded using the Otsu method (Otsu, 1979), to determine Red-positive and Red-negative areas within the cell. Next, the mean GFP fluorescence signal of these respective areas and from background pixels outside the identified cells was calculated. Figure 3b depicts these values and the pertinent standard error.

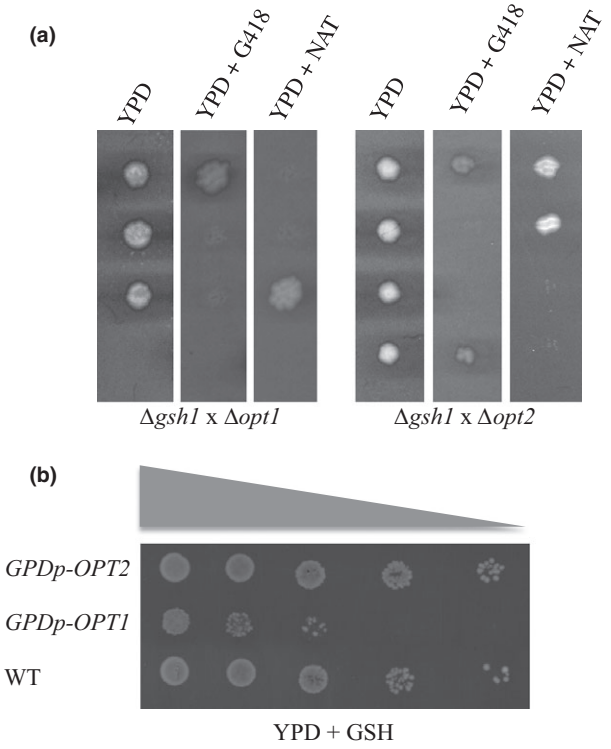

Fig. 1. The closely related proteins Opt1/Hgt1 and Opt2 display different glutathione-related phenotypes. (a) To uncover if Opt1 and Opt2 display similar glutathione-related phenotypes, we first crossed strains deleted for either *OPT1/HGT1* or *OPT2* with Δ*gsh1* cells, followed by sporulation and tetrad dissection. A representative tetrad for each cross is shown. No double mutant could be retrieved for the combination of Δ*opt1*/Δ*gsh1;* however, the double mutant Δ*opt2*/Δ*gsh1* could easily be recovered. Mutant identification was performed by replica plating on the selection medium assaying the expression of the selection cassette linked to each mutation. (b) We then serially diluted a control (WT) strain, or strains overexpressing either *OPT1/HGT1* or *OPT2* (*GPDp-OPT1*, *GPDp-OPT2*), and spotted them onto SD plates containing GSH (250 μM). Cells overexpressing Opt1, but not cells overexpressing Opt2, were hypersensitive to growth on high concentrations of GSH.

Glutathione measurements

Dynamic E_{GSH} measurements were made as described in detail previously (Morgan *et al.*, 2011). Essentially BY4742 (wildtype), Δ*opt2*, Δ*cta1*, Δ*opt2*/Δ*cta1*, and Δ*opt1* cells were transformed with either a p415 *TEFp* empty plasmid, p415 *TEFp* encoding Grx1-roGFP2, p415 *TEFp* encoding Grx1-roGFP2 with a C-terminal SKL sequence for peroxisomal targeting (Grx1-roGFP2-SKL) or p415 *TEFp* encoding Grx1-roGFP2 with an N-terminal mitochondrial targeting sequence derived from *Neurospora crassa* F0-ATPase subunit 9 protein (Su9-roGFP2-Grx1). Cells were grown in Hartwell's complete media lacking methionine and leucine, for 24 h at 25 °C. These precultures were used to inoculate fresh media at a 1 : 50 dilution and allowed to grow for a further 16 h at 25 °C for OD = 4 culture or 8 h for OD = 1 cultures. For each measurement, 4.5 OD_{600} units of cells were harvested by centrifugation at 800 ***g*** for 5 min and re-suspended into 600 μL 100 mM Mes/Tris pH 6.0. The re-suspended cells were divided into three 200 μL aliquots, one was treated with 20 mM diamide for a fully oxidized control, one with 100 mM DTT for the fully reduced control and the other left untreated to be used as the measured sample. All samples were transferred to a flat-bottomed 96-well plate and centrifuged for 5 min at 20 ***g*** to form a loose pellet in the bottom of the wells. Measurements were performed with a FLUOstar Omega plate-reader (BMG Labtech, Ortenberg, Germany), using excitation filters of 390/10 and 480/10 nm and recording emission at 510/10 nm. Measurements of the Su9-roGFP2-Grx1 probe in glucose grown cells were performed using a FP6500 spectrofluorimeter (Jasco) with constant stirring at 25 °C. Spectra were recorded with excitation wavelengths from 390–500 nm and an emission wavelength of 510 nm. Oxidation of the cytosolic glutathione pool was induced by the addition of H_2O_2 to a final concentration of 5 mM. The background corrected emission following excitation at both wavelengths was used to calculate the degree of probe oxidation (OxD roGFP2) according to Eqn. (1), where *I* is the background corrected fluorescence emission at 510 nm, following excitation at 390 or 480 nm, for the fully reduced (red) and fully oxidized (ox) controls and the experimental sample.

$$\mathrm{OxD}_{\mathrm{roGFP2}} = \frac{(I390\mathrm{sample} * I480\mathrm{red}) - (I390\mathrm{red} * I480\mathrm{sample})}{(I390\mathrm{sample} * I480\mathrm{red} - I390\mathrm{sample} * I480\mathrm{ox}) + (I390\mathrm{ox} * I480\mathrm{sample} - I390\mathrm{red} * I480\mathrm{sample})} \quad (1)$$

Whole cell glutathione determination

Whole cell GSH and GSSG concentration was determined using a modified version of the protocol described previously (Rahman *et al.*, 2006). Fifty OD_{600} units of cells were isolated by centrifugation, 1000 ***g***, 3 min at 25 °C, and washed once with 10 mL double distilled H_2O. Cells were again isolated by centrifugation and re-suspended in 250 μL 1.3% sulfosalicylic acid and 8 mM HCl (SSA buffer). Approximately, 500 μL of 0.5 mm acid-washed glass beads were added to the cell suspensions, and cells were broken by 3 min shaking with a Disruptor Genie cell homogenizer (Carl Roth GmbH & Co Karlsruhe, Germany) at 4 °C. A further 100 μL SSA buffer was added and samples disrupted for an additional 5 min. The resulting cell lysate was collected and incubated on ice for 15 min to precipitate protein, followed by 15 min centrifugation at 16 000 ***g***, 2 °C. Five microlitre of supernatant was removed immediately, diluted 1 : 100 in ice-cold potassium phosphate buffer pH 7.5 containing 5 mM EDTA (KPE buffer) and used for measurement of total glutathione. One hundred microlitre supernatant was incubated for 1 h at 25 °C with 2 μL 20% 2-vinylpyridine in ethanol and 40 μL 1 M Mes/Tris pH 7.0 to raise pH and alkylate GSH, thereby allowing determination of GSSG concentration. Samples were transferred to a 96-well flat-bottomed plate and treated by the addition of 110 μL KPE buffer containing 2 mg mL^{-1} NADPH and 2 mg mL^{-1} DTNB. Total glutathione and GSSG concentration were determined by measuring absorbance change at 412 nm following the addition of 50 μL KPE buffer containing 3.26 units mL^{-1} glutathione reductase (Sigma-Aldrich). Concentrations were determined by comparison to GSH and GSSG concentration standard curves. GSH concentration was determined by subtracting the GSSG concentration expressed as GSH equivalents from the total glutathione concentration.

Viability following H_2O_2 treatment

To assess the impact on cell viability of the H_2O_2 treatment employed during the E_{GSH} assay, we assayed the viability of WT yeast cells following H_2O_2 treatment under identical conditions. WT cells were resuspended to 7.5 OD_{600} units of cells mL^{-1} in 100 mM Mes/Tris pH 6.0. Cells were then either left untreated or treated with 5 mM H_2O_2 for 100 min. After treatment, cell suspensions were diluted and plated onto YPD agar plates in triplicate and incubated at 25 °C for 3 days, following which the mean number of colonies from the three replicate plates was determined. The experiment was repeated three times. The viability for each experiment was normalized to the mean of the untreated cells viability.

Results

The yeast OPT proteins display different GSH-related phenotypes

Oligopeptide transporters (OPTs) are a family of proteins conserved in plants and fungi (Wiles *et al.*, 2006; Gomolplitinant & Saier, 2011). Based on sequence similarity to the first characterized protein in this family as well as evidence from indirect transport experiments, they are predicted to transport small peptides across membranes (Lubkowitz *et al.*, 1997; Hauser *et al.*, 2000). The yeast *S. cerevisiae* Opt1/Hgt1 (High-affinity Glutathione Transporter 1) has been shown to function as a high-affinity PM glutathione/proton-coupled symporter (Bourbouloux *et al.*, 2000). In support of it being the major uptake system for GSH its deletion displays synthetic lethality with the glutathione biosynthetic pathway (Δ*gsh1*; Bourbouloux *et al.*, 2000; Fig. 1a, left panels).

Yeast contain an additional OPT family member, Opt2. As Opt2 is a close (60% similarity/30% identity of amino acids) homolog of Opt1 (Wiles *et al.*, 2006), we sought to determine if it shares redundant roles in transporting glutathione across the PM. First, we followed its synthetic lethality pattern with Δ*gsh1* and found that, in contrast to Δ*opt1*, a strain in which *OPT2* has been deleted does not display any synthetic effects (Fig. 1a, right panels). This is in line with previous data demonstrating that a Δ*opt2* strain is not deficient in taking up radiolabeled GSH into the cytosol (Bourbouloux *et al.*, 2000). Next, we found that whereas overexpression of Opt1 on the PM using a strong *GPD1* promoter caused cells to be hypersensitive to growth on high concentrations of GSH (Srikanth *et al.*, 2005), this was not the case for Opt2 (Fig. 1b). Taken together, our data indicate that Opt2 either has no role in glutathione transport under normal growth conditions, or that it is localized to a membrane other than the PM.

The two OPT family proteins localize to different cellular compartments

To assess whether the different phenotypes of the two family members may be a result of different subcellular localization, we first looked at strains from the systematic yeast green fluorescent protein (GFP) library where each yeast protein has been C-terminally tagged with GFP (Huh *et al.*, 2003). We found that Opt1-GFP was retained in the ER and was, therefore, incorrectly localized. The Opt2-GFP strain had no visible signal, which could be due to mis-folding or mis-targeting caused by the C-terminal GFP tag (data not shown and Huh *et al.*, 2003). To overcome this, we tagged each of the proteins with an

N-terminal GFP tag. The GFP-Opt1 protein localized to the PM as expected, while GFP-Opt2 localized to punctate intracellular structures (Fig. 2a). To determine the identity of the Opt2 containing structures, we performed co-localization analysis with a previously established panel of markers for cellular punctate structures, each tagged with a Red Fluorescent Protein (RFP; Huh *et al.*, 2003). Only the peroxisomal marker Pex3-RFP displayed full co-localization with the GFP-Opt2 fusion protein (Fig. 2b), indicating that Opt2 is a novel peroxisomal protein.

Peroxisomes in *S. cerevisiae* are crucial for the catabolism of a variety of molecules such as polyamines, purine bases, *n*-alkanes, and D-amino acids, as well as serving as the exclusive site of fatty acid beta-oxidation (Hiltunen *et al.*, 2003; Schrader & Fahimi, 2006). All of the above catabolic processes produce hydrogen peroxide (H_2O_2). In yeast, H_2O_2 can be broken down either by the peroxisomal catalase enzyme, Cta1 (Cohen *et al.*, 1988), or by the peroxisomal Glutathione Peroxidase, Gpx1 (Ohdate & Inoue, 2012). Gpx1 activity converts GSH to GSSG causing accumulation of GSSG that must be eliminated from peroxisomes. As a peroxisomal GSSG exporter was never identified, Opt2 became an obvious candidate for this role. Indeed, loss of Opt2 resulted in reduced ability to utilize oleic acid as a sole carbon source (Supporting Information, Fig. S1) indicative of reduced peroxisomal functions under conditions of increased H_2O_2 production and when peroxisomes become essential.

A peroxisomal-targeted glutathione sensor demonstrates that peroxisomes maintain a highly reduced glutathione pool

If indeed Opt2 functions in glutathione export, we would expect its absence to dramatically affect the reduced : oxidized ratio of the peroxisomal glutathione pool. roGFP2 has recently been used to measure the glutathione redox couple in peroxisomes (Ayer *et al.*, 2012). However, To equilibrate specifically with the glutathione redox couple, roGFP2 strictly requires the presence of a suitable glutaredoxin to catalyze the equilibration. Both yeast endogenous glutaredoxin 1 and 2 (Grx1 and Grx2) are able to fulfill this role (Morgan *et al.*, 2013). However, it is unknown whether they are present within the peroxisome and hence, whether roGFP2 really equilibrates with the glutathione redox couple in this compartment. To overcome this concern, we generated a peroxisome-targeted version of Grx1-roGFP2 (Gutscher *et al.*, 2008; Morgan *et al.*, 2011), which is a biosensor specific for the glutathione redox potential (E_{GSH}). Peroxisomal targeting was enabled by a C-terminal fusion of the three amino acids (SKL) comprising the strong peroxisomal targeting signal type 1 (PTS1; Gould *et al.*, 1989); and therefore, the probe is referred to as Grx1-roGFP2-SKL throughout the manuscript. We visually validated the correct targeting of Grx1-roGFP2-SKL by co-localization with the peroxisomal marker Pex3. The probe displayed robust peroxisomal localization (Fig. 3a and b) and had no deleterious

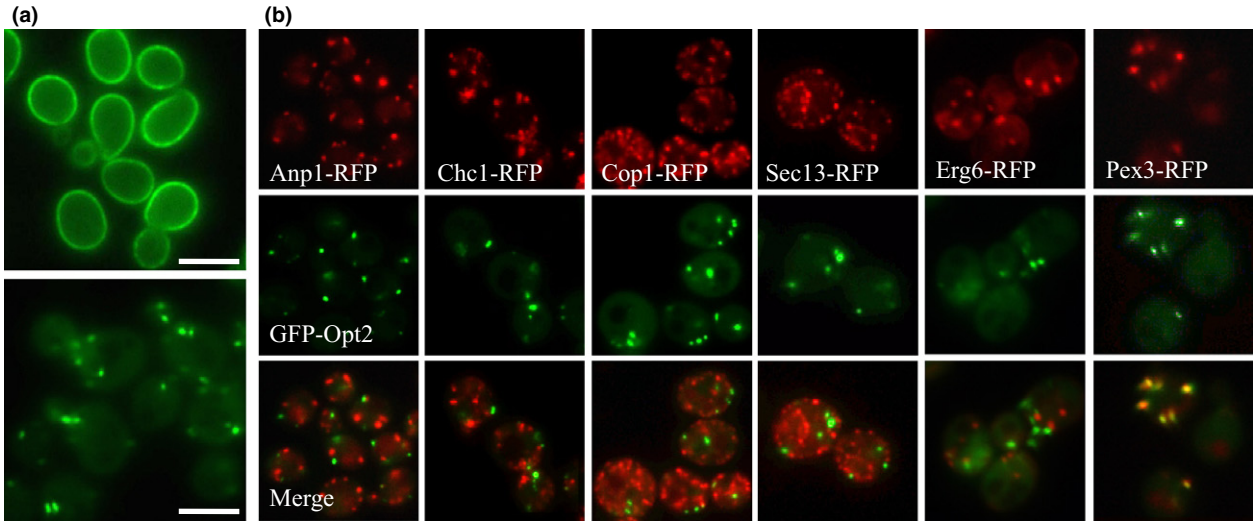

Fig. 2. Opt2 localizes to peroxisomes. (a) Representative images (scale bar = 5 μm) taken by fluorescence microscopy of strains expressing GFP-Opt1 (upper image) or GFP-Opt2 (lower image). GFP-Opt1 displayed PM localization, whereas GFP-Opt2 displayed punctate localization. (b) To characterize the punctate structures to which Opt2 is localized, we co-expressed RFP-tagged proteins marking different intracellular punctuate structures (Anp1: Golgi; Chc1: late Golgi; Cop1: Golgi to ER vesicles; Sec13: ER to Golgi vesicles, Erg6: lipid droplets; Pex3: peroxisomes) in GFP-Opt2 strain. Using these markers, we found that GFP-Opt2 is co-localized solely with Pex3-RFP.

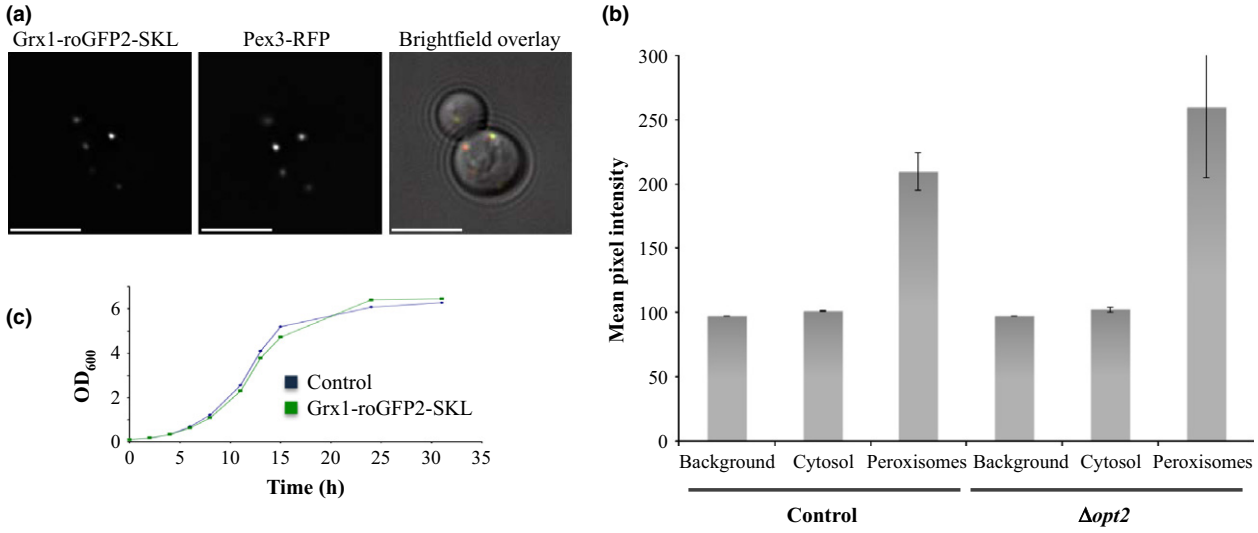

Fig. 3. The Grx1-roGFP2-SKL sensor localizes to peroxisomes. (a) To examine the localization of the Grx1-roGFP2-SKL probe, we transformed cells expressing Pex3-RFP with a plasmid encoding the roGFP2-SKL probe. Representative images (Scale bar = 5 μm) demonstrate a perfect co-localization pattern. (b) We further transformed control or Δ*opt2* cells expressing Pex3-RFP/cherry with a plasmid encoding the roGFP2-SKL probe, and measured the mean pixel intensity in background pixels, Pex3-RFP/cherry-negative (cytosol), and Pex3-RFP/cherry-positive (peroxisomes) regions. The mean signal in the GFP-channel was significantly higher in the Red-positive region than in the Red-negative region that had mean pixel intensity similar to the background. This result suggests that the probe was targeted to peroxisomes with high fidelity, and hence, exclusively reports E_{GSH} from inside this organelle. (c) To examine if the Grx1-roGFP2-SKL affects cell growth, control cells (BY4742) or cells expressing Grx1-roGFP2-SKL were grown. Identical growth curves demonstrate that the probe did not lead to any change in fitness.

effect on cell growth (Fig. 3c). Using this probe and assuming a pH of 7.0, we then measured E_{GSH} in the peroxisomal matrix as being -319 ± 7 mV in a WT strain, which is very similar to recently reported values for the cytosol, mitochondrial intermembrane space and mitochondrial matrix (Morgan *et al.*, 2011; Kojer *et al.*, 2012). The peroxisomal matrix in yeast was recently measured to be pH 8.0 (Ayer *et al.*, 2012). Correcting for pH, yields an E_{GSH} of *c.* −380 mV. This is considerably more reducing than reported by Ayer *et al.*, and indicates that indeed Grx activity is absent or is limited in the peroxisomal matrix and thus roGFP2 alone, that is without a genetically fused Grx moiety, might not accurately report E_{GSH} in this compartment.

Deletion of *OPT2* affects peroxisomal glutathione redox homeostasis

To investigate the role of Opt2 in peroxisomal glutathione redox homeostasis, we expressed the peroxisomal probe in cells deleted for *OPT2* and measured the ability to re-normalize E_{GSH} following an acute challenge with the oxidant H_2O_2 (Fig. 4a). Importantly, the H_2O_2 challenge had no significant effect on cell viability (Fig. S2). Because peroxisomal catalase (Cta1) is the parallel pathway for the removal of H_2O_2 in this organelle, we also investigated the consequences of deleting *CTA1* either alone or in combination with *OPT2* for peroxisomal glutathione redox homeostasis.

The loss of Opt2 had dramatic effects: the peroxisomal glutathione pool became more oxidized than in a WT strain following the H_2O_2 challenge, and in the course of the experiment never returned to basal levels (Fig. 4a) consistent with inability of the peroxisome to excrete GSSG. In contrast, the loss of peroxisomal catalase had no significant effect on the recovery of the peroxisomal glutathione pool following an H_2O_2 challenge. This seems surprising considering the enzymatic function of Cta1 in detoxifying H_2O_2, although it is in line with previous observations that the Δ*cta1* mutant is still able to grow in the presence of fatty acids as sole carbon source – conditions in which H_2O_2 levels are believed to be elevated (Hiltunen *et al.*, 2003). One possible explanation for this finding is that under normal growth condition it is the glutathione peroxidase activity in this compartment that takes on the majority of H_2O_2 breakdown. However, the double mutant Δ*cta1*/Δ*opt2* had the most severe phenotype – reaching the sensitivity limit of the probe in the extent of glutathione pool oxidation and showing complete inability to re-establish homeostasis within the experimental time frame.

Interestingly, the ability of peroxisomes to re-establish glutathione redox homeostasis and the effect of Cta1 and Opt2 were independent of growth phase (pre- and post-

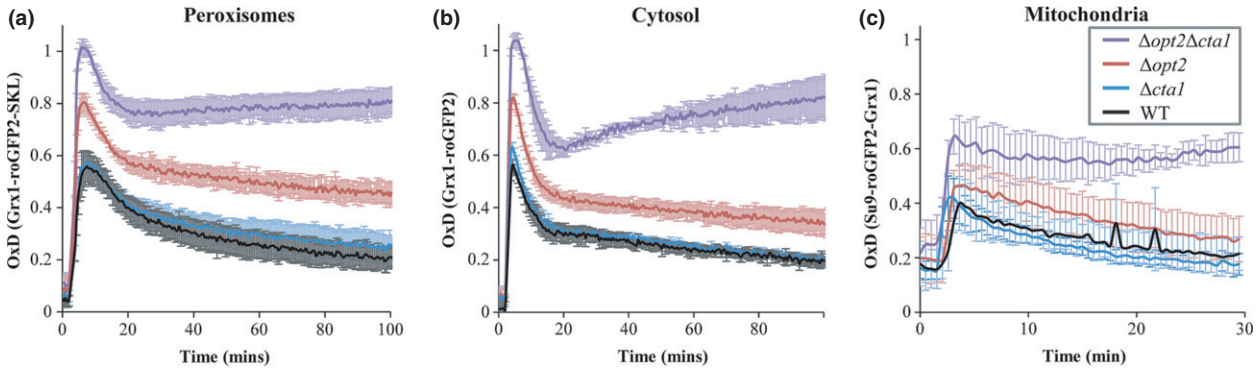

Fig. 4. Deletion of OPT2 impairs peroxisomal, cytosolic, and mitochondrial glutathione homeostasis. To uncover the effect of loss of Opt2 and Cta1 on peroxisomal (a), cytosolic (b), and mitochondrial (c) glutathione homeostasis, we transformed WT, Δ*cta1*, Δ*opt2,* and Δ*cta1*/Δ*opt2* with control vector or with plasmids expressing Grx1-roGFP2-SKL (peroxisomal), Grx1-roGFP2 (cytosolic), or Su9-roGFP2-Grx1 (mitochondrial) GSH probes. We then measured the response of the different sensors in cells at OD_{600} = 4 to the addition of 5 mM H_2O_2 (n = 3). The results show loss of *OPT2* affects peroxisomal, cytosolic, and mitochondrial glutathione homeostasis, and that loss of *OPT2* in combination with loss of *CTA1* had a synthetic effect.

diauxic shift, OD = 1 and OD = 4, respectively; see Fig. 4a for OD = 4 and Fig. S3a for OD = 1).

Together, these findings support the notion that Cta1 and Opt2 independently and additively affect peroxisomal glutathione redox homeostasis.

Loss of Opt2 affects cytosolic glutathione redox homeostasis

As deletion of *OPT2* dramatically affected peroxisomal glutathione homeostasis, we sought to determine whether it also affects cytosolic homeostasis. We used the cytosolic Grx1-roGFP2 probe to measure the changes in cytosolic E_{GSH}, in the same genetic backgrounds (Fig. 4b). Strikingly, the cytosolic glutathione pool was affected to a similar extent as the peroxisome by the deletion of *OPT2*. Interestingly, we observed that following 100 min of H_2O_2 challenge, whole cell GSH was slightly reduced whereas whole cell GSSG was increased in Δ*opt2* cells compared to WT cells (Fig. S4a and b). These data demonstrate that cellular glutathione homeostasis is impaired when OPT2 is lost. In addition, they suggest that in the absence of Opt2 the cell has an overall reduced ability to convert GSSG to GSH.

Loss of Opt2 affects mitochondrial function

The glutathione pool in the mitochondrial matrix is known to be relatively isolated from the cytosolic glutathione pool. Changes in the redox state of the cytosolic and mitochondrial matrix glutathione pools can occur independently of each other (Kojer *et al.*, 2012). However, a complicated interplay between peroxisomal and mitochondrial redox processes has recently been reported (Ivashchenko *et al.*, 2011). Therefore, we also investigated the effect of *OPT2* deletion on the capacity of mitochondrial glutathione pool to resist an oxidative challenge with H_2O_2. We targeted roGFP2-Grx1 to the mitochondrial matrix by the fusion of the targeting sequence of *N. crassa* F0-ATPase subunit 9 (Su9-roGFP2-Grx1) (Kojer *et al.*, 2012). Similar to the cytosol and peroxisomal lumen, we observed that OPT2 deletion led to a reduced ability to restore glutathione redox homoestasis in the mitochondrial matrix following challenge with exogenously applied H_2O_2 (Fig. 4c). Thus, *OPT2* deletion apparently leads to a cell-wide defect in glutathione homeostasis, affecting at least three major cellular compartments.

As Opt2 obviously had dramatic effects on cellular glutathione homeostasis, we wanted to obtain a broader view of the cellular processes that might be affected by the loss of *OPT2*. To assess which processes would be most affected by an *OPT2* deletion, we performed a synthetic lethality screen of Δ*opt2* against the entire yeast deletion library (Giaever *et al.*, 2002), either under normal growth conditions or under conditions of oxidative stress (growth in the presence of diamide). Strikingly, the genes synthetically lethal with Δ*opt2* were highly enriched for mitochondrial proteins (Table 2 (http://yeastmine.yeastgenome.org/yeastmine p=0.01). In addition, under conditions of oxidative stress, we identified a number of genes essential for iron metabolism (*FET3*, *SIT1*, *ARR3*, *GEF1*). Both, the multi-copper oxidase Fet3 and the endosomal CLC chloride-proton exchanger Gef1 are required for cells to grow under iron limitation (Davis-Kaplan *et al.*, 1998). These results are consistent with recent measurements, also employing the Grx1-roGFP2 probe, which demonstrated that deletion of *GEF1*, a gene encoding a chloride-proton antiporter that is essential for

Table 2. Synthetic lethality screen results

ORF	Gene name	GO description	Phenotype
YBR163W	EXO5	Mitochondrial 5′–3′ exonuclease and sliding exonuclease, required for mitochondrial genome maintenance, distantly related to the RecB nuclease domain of bacterial RecBCD recombinases, may be regulated by the transcription factor Ace2	Growth defect
YDL202W	MRPL11	Mitochondrial ribosomal protein of the large subunit	Growth defect
YDR268W	MSW1	Mitochondrial tryptophanyl-tRNA synthetase	Growth defect
YDR512C	EMI1	Nonessential protein required for transcriptional induction of the early meiotic-specific transcription factor IME1, also required for sporulation, contains twin cysteine-x9-cysteine motifs	Growth defect
YEL064C	AVT2	Putative transporter, member of a family of seven *S. cerevisiae* genes (AVT1-7) related to vesicular GABA-glycine transporters	Growth defect
YEL065W	SIT1	Ferrioxamine B transporter, member of the ARN family of transporters that specifically recognize siderophore-iron chelates; transcription is induced during iron deprivation and diauxic shift, potentially phosphorylated by Cdc28p	Synthetic lethal
YER087W	AIM10	Protein with similarity to tRNA synthetases; nontagged protein is detected in purified mitochondria; null mutant is viable and displays elevated frequency of mitochondrial genome loss	Synthetic lethal
YER177W	BMH1	14-3-3 protein, major isoform, controls proteome at post-transcriptional level, binds proteins and DNA, involved in regulation of many processes including exocytosis, vesicle transport, Ras/MAPK signaling, and rapamycin-sensitive signaling	Growth defect
YER178W	PDA1	E1 alpha subunit of the pyruvate dehydrogenase complex catalyzes the direct oxidative decarboxylation of pyruvate to acetyl-CoA, phosphorylated, regulated by glucose	Synthetic lethal
YGL133W	ITC1	Subunit of the ATP-dependent Isw2p-Itc1p chromatin remodeling complex, required for repression of a specific genes, repression of early meiotic genes during mitotic growth, and repression of INO1; similar to mammalian Acf1p, the regulatory subunit of the mammalian ATP-utilizing chromatin assembly and modifying factor (ACF) complex	Growth defect
YGL136C	MRM2	Mitochondrial 2′ O-ribose methyltransferase required for methylation of U(2791) in 21S rRNA; MRM2 deletion confers thermosensitive respiration and loss of mitochondrial DNA, has similarity to Spb1p and Trm7p, and to *E. coli* FtsJ/RrmJ	Growth defect
YGL143C	MRF1	Mitochondrial translation release factor, involved in stop codon recognition and hydrolysis of the peptidyl-tRNA bond during mitochondrial translation; lack of MRF1 causes mitochondrial genome instability	Synthetic lethal
YGR076C	MRPL25	Mitochondrial ribosomal protein of the large subunit	Growth defect
YGR214W	RPS0A	Protein component of the small (40S) ribosomal subunit, nearly identical to Rps0Bp, required for maturation of 18S rRNA along with Rps0Bp; deletion of either RPS0 gene reduces growth rate, deletion of both genes is lethal	Growth defect
YGR219W	Overlaps MRPL9	MRPL9 is mitochondrial ribosomal protein of the large subunit	Synthetic lethal
YGR285C	ZUO1	Ribosome-associated chaperone, functions in ribosome biogenesis and, in partnership with Ssz1p and SSb1/2, as a chaperone for nascent polypeptide chains contains a DnaJ domain and functions as a J-protein partner for Ssb1p and Ssb2p	Synthetic lethal
YHR178W	STB5	Transcription factor, involved in regulating multidrug resistance and oxidative stress response, forms a heterodimer with Pdr1p and contains a Zn(II)2Cys6 zinc finger domain that interacts with a pleiotropic drug resistance element *in vitro*	Growth defect
YIL052C	RPL34B	Protein component of the large (60S) ribosomal subunit, nearly identical to Rpl34Ap and has similarity to rat L34 ribosomal protein	Synthetic lethal
YIL110W	HPM1	AdoMet-dependent methyltransferase involved in a novel 3-methylhistidine modification of ribosomal protein Rpl3p; seven beta-strand MTase family member; null mutant exhibits a weak vacuolar protein sorting defect and caspofungin resistance	Synthetic lethal
YJL004C	SYS1	Integral membrane protein of the Golgi required for targeting of the Arf-like GTPase Arl3p to the Golgi; multicopy suppressor of ypt6 null mutation	Growth defect
YJL189W	RPL39	Protein component of the large (60S) ribosomal subunit has similarity to rat L39 ribosomal protein, required for ribosome biogenesis and loss of both Rpl31p; Rpl39p confers lethality and also exhibits genetic interactions with SIS1 and PAB1	Synthetic lethal
YJR040W	GEF1	Voltage-gated chloride channel localized to the golgi, the endosomal system, and plasma membrane (PM) and involved in cation homeostasis; highly homologous to vertebrate voltage-gated chloride channels	Synthetic lethal

Table 2. Continued

ORF	Gene name	GO description	Phenotype
YKL170W	MRPL38	Mitochondrial ribosomal protein of the large subunit appears as two protein spots (YmL34 and YmL38) on two-dimensional SDS gels	Growth defect
YKR085C	MRPL20	Mitochondrial ribosomal protein of the large subunit	Growth defect
YLR182W	SWI6	Transcription cofactor forms complexes with Swi4p and Mbp1p to regulate transcription at the G1/S transition involved in meiotic gene expression; cell wall stress induces phosphorylation by Mpk1p, which regulates Swi6p localization	Synthetic lethal
YLR239C	LIP2	Lipoyl ligase involved in the modification of mitochondrial enzymes by the attachment of lipoic acid groups	Synthetic lethal
YMR058W	FET3	Ferro-O2-oxidoreductase required for high-affinity iron uptake and involved in mediating resistance to copper ion toxicity belongs to class of integral membrane multicopper oxidases	Synthetic lethal
YNL055C	POR1	Mitochondrial porin (voltage-dependent anion channel), outer-membrane protein required for the maintenance of mitochondrial osmotic stability and mitochondrial membrane permeability; phosphorylated	Growth defect
YNL265C	IST1	Protein with a positive role in the multivesicular body sorting pathway functions and forms a complex with Did2p; recruitment to endosomes is mediated by the Vps2p-Vps24p subcomplex of ESCRT-III and also interacts with Vps4p	Synthetic lethal
YOR275C	RIM20	Protein involved in proteolytic activation of Rim101p in response to alkaline pH; PalA/AIP1/Alix family member; interaction with the ESCRT-III subunit Snf7p suggests a relationship between pH response and multivesicular body formation	Growth defect
YOR369C	RPS12	Protein component of the small (40S) ribosomal subunit has similarity to rat ribosomal protein S12	Growth defect
YPL173W	MRPL40	Mitochondrial ribosomal protein of the large subunit	Growth defect
YPR047W	MSF1	Mitochondrial phenylalanyl-tRNA synthetase, active as a monomer, unlike the cytoplasmic subunit which is active as a dimer complexed to a beta subunit dimer; similar to the alpha subunit of *E. coli* phenylalanyl-tRNA synthetase	Growth defect
YPR173C	VPS4	AAA-ATPase involved in multivesicular body (MVB) protein sorting, ATP-bound Vps4p localizes to endosomes and catalyzes ESCRT-III disassembly and membrane release; ATPase activity is activated by Vta1p and regulates cellular sterol metabolism	Synthetic lethal
YPR201W	ARR3	PM metalloid/H+ antiporter transports arsenite and antimonite, required for resistance to arsenic compounds; transcription is activated by Arr1p in the presence of arsenite	Growth defect

Results in red represent synthetic lethal interactions observed in both normal and oxidative stress conditions. All other results displayed synthetic lethal interactions only under oxidative stress conditions.

high-affinity iron uptake, significantly impacted upon cytosolic glutathione redox homeostasis, particularly following a challenge with exogenously applied H_2O_2 (Braun *et al.*, 2010).

Conclusions

Our work demonstrates that Opt2, a close homolog of the known glutathione transporter Opt1, localizes to peroxisomes. Additionally, we created a peroxisome-targeted E_{GSH} probe that allowed us the investigation of the effects of specific proteins on peroxisomal glutathione redox homeostasis. The use of this probe in combination with Grx1-roGFP2 probes targeted to the cytosol and mitochondrial matrix allowed us to demonstrate that loss of Opt2 led to a cell-wide disruption of glutathione homeostasis following a challenge with exogenously applied H_2O_2.

We further performed a synthetic lethality screen of Δ*opt2* against the entire yeast deletion library and found enrichment for mitochondrial proteins. In addition, we identified several genes essential for iron metabolism under conditions of oxidative stress. These results suggest that iron-sulfur cluster biogenesis is the mitochondrial function that is most affected by the disturbance of glutathione homeostasis in a Δ*opt2* strain. Interestingly, lipoate synthase, which provides lipoic acid modifications to a small group of specific enzymes, including the E2 subunits of pyruvate dehydrogenase (PDH), is an iron-sulfur protein (Lill, 2009). Because loss of both the lipoic acid pathway and PDH were synthetic lethal with Δ*opt2*, an appealing explanation for the dependence on iron metabolism is that in the absence of a functional TCA cycle it is essential that peroxisomes function optimally in beta-oxidation of fatty acids to produce enough energy for yeast growth. In support of this, we have recently shown that peroxisomes are juxtaposed to sites of PDH complex accumulation suggesting that cross talk and coordination may occur at such sites (Cohen *et al.*, 2014). Moreover, several recent publications point to a coordination between peroxisomal proteins and cellular iron metabolism. For example, a recent study combining mutant and

transcriptome analyses to identify novel genes important for cellular iron homeostasis, found a highly significant enrichment of peroxisomal proteins, as well as proteins involved in peroxisome biogenesis and peroxisomal protein targeting (Jo *et al.*, 2009). Furthermore, it was reported that deletion of the gene encoding peroxisomal citrate synthase *CIT2* attenuated the impact of deleting the key mitochondrial iron homeostasis proteins, the frataxin homolog *YFH1* (Chen *et al.*, 2002).

Based on its homology to Opt1 and its effect on glutathione homeostasis, we suggest that the peroxisomal protein, Opt2, is transporting a species of glutathione. Notably, the mammalian peroxisomal membrane is freely permeable to small metabolites with molecular masses lower than 300 Da. Therefore, it was previously suggested that GSH (*c.* 300 Da) may easily diffuse across the peroxisomal membrane, but the heavier, oxidized form, GSSG (*c.* 600 Da), will not. In addition, it was suggested that mammalian peroxisomes eliminate GSSG by a mechanism that is not dependent on glutathione reductase activity but rather by specific membrane transporters whose identity remains unknown (Antonenkov & Hiltunen, 2006). Assuming conservation of these traits in yeast and alongside our data showing that both peroxisomal and whole cell GSSG are increased upon H_2O_2 challenge, one potential function of Opt2 may be to transport GSSG out of peroxisomes. However, both the direction of transport as well as the transported molecule of Opt2 remain to be uncovered. Our work opens new possibilities to study the role of peroxisomes in glutathione homeostasis and how different subcellular compartments communicate with each other to maintain cellular redox homeostasis.

Acknowledgements

B.S. and A.C. were supported by a Wellcome Trust Senior Research Fellowship to B.S. M.S. and Y.E. were supported by an ERC StG (260395). T.P.D. is supported by grants from the DFG (SFB 1036, SPP 1710). B.M. was supported by a Visiting Scientist Fellowship from the German Cancer Research Center. We thank Jan Riemer (University of Kaiserslautern) for help with spectrofluorimetry.

Authors' contribution

Y.E and B.M contributed equally to this work. M.S., B.S. and T.P.D. are equal senior authors.

Statement

(1) Opt2, a homolog of the Opt1 glutathione transporter, is localized to peroxisomes.
(2) We created a new probe for measuring the glutathione redox potential in peroxisomes.
(3) Loss of Opt2 affects glutathione redox homeostasis in peroxisomes, mitochondria, and the cytosol.

References

Antonenkov VD & Hiltunen JK (2006) Peroxisomal membrane permeability and solute transfer. *Biochim Biophys Acta* **1763**: 1697–1706.

Ayer A, Fellermeier S, Fife C, Li SS, Smits G, Meyer AJ, Dawes IW & Perrone GG (2012) A genome-wide screen in yeast identifies specific oxidative stress genes required for the maintenance of sub-cellular redox homeostasis. *PLoS ONE* **7**: e44278.

Birk J, Meyer M, Aller I, Hansen HG, Odermatt A, Dick TP, Meyer AJ & Appenzeller-Herzog C (2013) Endoplasmic reticulum: reduced and oxidized glutathione revisited. *J Cell Sci* **126**: 1604–1617.

Bourbouloux A, Shahi P, Chakladar A, Delrot S & Bachhawat AK (2000) Hgt1p, a high affinity glutathione transporter from the yeast *Saccharomyces cerevisiae*. *J Biol Chem* **275**: 13259–13265.

Brachmann CB, Davies A, Cost GJ, Caputo E, Li J, Hieter P & Boeke JD (1998) Designer deletion strains derived from *Saccharomyces cerevisiae* S288C: a useful set of strains and plasmids for PCR-mediated gene disruption and other applications. *Yeast* **14**: 115–132.

Braun NA, Morgan B, Dick TP & Schwappach B (2010) The yeast CLC protein counteracts vesicular acidification during iron starvation. *J Cell Sci* **123**: 2342–2350.

Breslow DK, Cameron DM, Collins SR, Schuldiner M, Stewart-Ornstein J, Newman HW, Braun S, Madhani HD, Krogan NJ & Weissman JS (2008) A comprehensive strategy enabling high-resolution functional analysis of the yeast genome. *Nat Methods* **5**: 711–718.

Chen OS, Hemenway S & Kaplan J (2002) Genetic analysis of iron citrate toxicity in yeast: implications for mammalian iron homeostasis. *P Natl Acad Sci USA* **99**: 16922–16927.

Cohen Y & Schuldiner M (2011) Advanced methods for high-throughput microscopy screening of genetically modified yeast libraries. *Methods Mol Biol* **781**: 127–159.

Cohen G, Rapatz W & Ruis H (1988) Sequence of the *Saccharomyces cerevisiae* CTA1 gene and amino acid sequence of catalase A derived from it. *Eur J Biochem* **176**: 159–163.

Cohen Y, Klug YA, Dimitrov L *et al.* (2014) Peroxisomes are juxtaposed to strategic sites on mitochondria. *Mol BioSyst* **10**: 1742–1748.

Dardalhon M, Kumar C, Iraqui I *et al.* (2012) Redox-sensitive YFP sensors monitor dynamic nuclear and cytosolic glutathione redox changes. *Free Radic Biol Med* **52**: 2254–2265.

Davis-Kaplan SR, Askwith CC, Bengtzen AC, Radisky D & Kaplan J (1998) Chloride is an allosteric effector of copper assembly for the yeast multicopper oxidase Fet3p: an

unexpected role for intracellular chloride channels. *P Natl Acad Sci USA* **95**: 13641–13645.
Dhaoui M, Auchere F, Blaiseau PL, Lesuisse E, Landoulsi A, Camadro JM, Haguenauer-Tsapis R & Belgareh-Touze N (2011) Gex1 is a yeast glutathione exchanger that interferes with pH and redox homeostasis. *Mol Biol Cell* **22**: 2054–2067.
Giaever G, Chu AM, Ni L *et al.* (2002) Functional profiling of the *Saccharomyces cerevisiae* genome. *Nature* **418**: 387–391.
Gietz RD & Woods RA (2006) Yeast transformation by the LiAc/SS carrier DNA/PEG method. *Methods Mol Biol* **313**: 107–120.
Gomolplitinant KM & Saier MH Jr (2011) Evolution of the oligopeptide transporter family. *J Membr Biol* **240**: 89–110.
Gould SJ, Keller GA, Hosken N, Wilkinson J & Subramani S (1989) A conserved tripeptide sorts proteins to peroxisomes. *J Cell Biol* **108**: 1657–1664.
Grant CM (2001) Role of the glutathione/glutaredoxin and thioredoxin systems in yeast growth and response to stress conditions. *Mol Microbiol* **39**: 533–541.
Grant CM, MacIver FH & Dawes IW (1996) Glutathione is an essential metabolite required for resistance to oxidative stress in the yeast *Saccharomyces cerevisiae*. *Curr Genet* **29**: 511–515.
Gutscher M, Pauleau AL, Marty L, Brach T, Wabnitz GH, Samstag Y, Meyer AJ & Dick TP (2008) Real-time imaging of the intracellular glutathione redox potential. *Nat Methods* **5**: 553–559.
Hauser M, Donhardt AM, Barnes D, Naider F & Becker JM (2000) Enkephalins are transported by a novel eukaryotic peptide uptake system. *J Biol Chem* **275**: 3037–3041.
Herrero E, Ros J, Belli G & Cabiscol E (2008) Redox control and oxidative stress in yeast cells. *Biochim Biophys Acta* **1780**: 1217–1235.
Hiltunen JK, Mursula AM, Rottensteiner H, Wierenga RK, Kastaniotis AJ & Gurvitz A (2003) The biochemistry of peroxisomal beta-oxidation in the yeast *Saccharomyces cerevisiae*. *FEMS Microbiol Rev* **27**: 35–64.
Huh WK, Falvo JV, Gerke LC, Carroll AS, Howson RW, Weissman JS & O'Shea EK (2003) Global analysis of protein localization in budding yeast. *Nature* **425**: 686–691.
Ivashchenko O, Van Veldhoven PP, Brees C, Ho YS, Terlecky SR & Fransen M (2011) Intraperoxisomal redox balance in mammalian cells: oxidative stress and interorganellar cross-talk. *Mol Biol Cell* **22**: 1440–1451.
Janke C, Magiera MM, Rathfelder N *et al.* (2004) A versatile toolbox for PCR-based tagging of yeast genes: new fluorescent proteins, more markers and promoter substitution cassettes. *Yeast* **21**: 947–962.
Jo WJ, Kim JH, Oh E, Jaramillo D, Holman P, Loguinov AV, Arkin AP, Nislow C, Giaever G & Vulpe CD (2009) Novel insights into iron metabolism by integrating deletome and transcriptome analysis in an iron deficiency model of the yeast *Saccharomyces cerevisiae*. *BMC Genomics* **10**: 130.
Jonikas MC, Collins SR, Denic V *et al.* (2009) Comprehensive characterization of genes required for protein folding in the endoplasmic reticulum. *Science* **323**: 1693–1697.
Klein M, Mamnun YM, Eggmann T, Schuller C, Wolfger H, Martinoia E & Kuchler K (2002) The ATP-binding cassette (ABC) transporter Bpt1p mediates vacuolar sequestration of glutathione conjugates in yeast. *FEBS Lett* **520**: 63–67.
Kojer K, Bien M, Gangel H, Morgan B, Dick TP & Riemer J (2012) Glutathione redox potential in the mitochondrial intermembrane space is linked to the cytosol and impacts the Mia40 redox state. *EMBO J* **31**: 3169–3182.
Kumar C, Igbaria A, D'Autreaux B, Planson AG, Junot C, Godat E, Bachhawat AK, Delaunay-Moisan A & Toledano MB (2011) Glutathione revisited: a vital function in iron metabolism and ancillary role in thiol-redox control. *EMBO J* **30**: 2044–2056.
Li ZS, Szczypka M, Lu YP, Thiele DJ & Rea PA (1996) The yeast cadmium factor protein (YCF1) is a vacuolar glutathione S-conjugate pump. *J Biol Chem* **271**: 6509–6517.
Lill R (2009) Function and biogenesis of iron-sulphur proteins. *Nature* **460**: 831–838.
Longtine MS, McKenzie A III, Demarini DJ, Shah NG, Wach A, Brachat A, Philippsen P & Pringle JR (1998) Additional modules for versatile and economical PCR-based gene deletion and modification in *Saccharomyces cerevisiae*. *Yeast* **14**: 953–961.
Lopez-Mirabal HR & Winther JR (2008) Redox characteristics of the eukaryotic cytosol. *Biochim Biophys Acta* **1783**: 629–640.
Lubkowitz MA, Hauser L, Breslav M, Naider F & Becker JM (1997) An oligopeptide transport gene from *Candida albicans*. *Microbiology* **143**(Pt 2): 387–396.
Meister A (1988) Glutathione metabolism and its selective modification. *J Biol Chem* **263**: 17205–17208.
Meyer AJ & Dick TP (2010) Fluorescent protein-based redox probes. *Antioxid Redox Signal* **13**: 621–650.
Morgan B, Sobotta MC & Dick TP (2011) Measuring E(GSH) and H2O2 with roGFP2-based redox probes. *Free Radic Biol Med* **51**: 1943–1951.
Morgan B, Ezerina D, Amoako TN, Riemer J, Seedorf M & Dick TP (2013) Multiple glutathione disulfide removal pathways mediate cytosolic redox homeostasis. *Nat Chem Biol* **9**: 119–125.
Ohdate T & Inoue Y (2012) Involvement of glutathione peroxidase 1 in growth and peroxisome formation in *Saccharomyces cerevisiae* in oleic acid medium. *Biochim Biophys Acta* **1821**: 1295–1305.
Otsu N (1979) A threshold selection method from gray-level histograms. *IEEE Trans Syst Man Cybern* **9**: 62–66.
Rahman I, Kode A & Biswas SK (2006) Assay for quantitative determination of glutathione and glutathione disulfide levels using enzymatic recycling method. *Nat Protoc* **1**: 3159–3165.
Rebbeor JF, Connolly GC, Dumont ME & Ballatori N (1998) ATP-dependent transport of reduced glutathione on YCF1, the yeast orthologue of mammalian multidrug resistance associated proteins. *J Biol Chem* **273**: 33449–33454.
Schrader M & Fahimi HD (2006) Growth and division of peroxisomes. *Int Rev Cytol* **255**: 237–290.
Sharma KG, Mason DL, Liu G, Rea PA, Bachhawat AK & Michaelis S (2002) Localization, regulation, and substrate

transport properties of Bpt1p, a *Saccharomyces cerevisiae* MRP-type ABC transporter. *Eukaryot Cell* **1**: 391–400.
Srikanth CV, Vats P, Bourbouloux A, Delrot S & Bachhawat AK (2005) Multiple cis-regulatory elements and the yeast sulphur regulatory network are required for the regulation of the yeast glutathione transporter, Hgt1p. *Curr Genet* **47**: 345–358.
Tiwari A & Sekhar AK (2007) Workflow based framework for life science informatics. *Comput Biol Chem* **31**: 305–319.
Tong AH & Boone C (2006) Synthetic genetic array analysis in *Saccharomyces cerevisiae*. *Methods Mol Biol* **313**: 171–192.
Tong AH, Evangelista M, Parsons AB *et al.* (2001) Systematic genetic analysis with ordered arrays of yeast deletion mutants. *Science* **294**: 2364–2368.
Wiles AM, Naider F & Becker JM (2006) Transmembrane domain prediction and consensus sequence identification of the oligopeptide transport family. *Res Microbiol* **157**: 395–406.

Supporting Information

Additional Supporting Information may be found in the online version of this article:

Fig. S1. Loss of *OPT2* reduces the ability to utilize oleic acid as a sole carbon source.
Fig. S2. Five millimolar H_2O_2 does not affect cell viability.
Fig. S3. Deletion of *OPT2* impairs glutathione homeostasis also in logarithmically growing cells.
Fig. S4. Deletion of *OPT2* affects overall cellular glutathione levels following H_2O_2 challenge.